Thesis for the Degree of Licentiate of Engineering

Characterization and Compensation of Thermal Effects in GaN HEMT Technologies

Johan Bremer

CHALMERS

Microwave Electronics Laboratory
Department of Microtechnology and Nanoscience – MC2
Chalmers University of Technology
Göteborg, Sweden 2020

Characterization and Compensation of Thermal Effects in GaN HEMT Technologies

Johan Bremer

Chalmers University of Technology
Department of Microtechnology and Nanoscience – MC2
Microwave Electronics Laboratory
SE-412 96 Göteborg, Sweden
+ 46 (0) 31-772 1000

ISSN 1652-0769
Technical report MC2-429

Printed by Chalmers Reproservice
Göteborg, Sweden 2020

Abstract

Further advancements with GaN based technologies relies on the ability to handle the heat flux, which consequently arises from the high power density. Advanced cooling techniques and thermal optimization of the technology are therefore prioritized research areas. Characterization techniques play a key role in the development of new cooling solutions, since these rely on accurate measurements of e.g. the temperature of the device. This thesis covers techniques to electrically characterize the lateral and vertical heat properties in GaN, and a temperature compensation technique for GaN MMICs.

The first part outlines a methodology to electrically extract the thermal resistance of a GaN resistor without risking distortion from field induced electron trapping effects, which are exhibited by GaN heterostructures. The technique uses differential resistance measurements to identify a suitable resistor geometry, which minimizes trapping effects while enhancing the self-heating. Such conditions are crucial for electrical methods since these exploit the self-heating for a thermal analysis.

Furthermore, a test structure and measurement method to electrically characterize the lateral heat spread was designed and evaluated. The structure is implemented with a thermal sensor, which utilizes the temperature-dependent IV characteristics of a GaN resistor, making it suitable for integration in GaN MMICs. The transient response can be obtained to extract the thermal time constants and propagation delay of the heat spread. At higher ambient temperatures, the propagation delay increases and the thermal coupling is increased.

Lastly, a biasing technique to compensate for thermal degradation of the RF performance of an LNA was developed. By utilizing the gate- and drain voltage dependence of the RF performance, a constant gain against increasing temperature can e.g. be achieved.

Keywords: characterization, AlGaN/GaN, thermal effects, electrothermal, thermal resistance, thermal coupling, temperature compensation.

List of Publications

Appended Publications

This thesis is based on work contained in the following papers:

[A] J. Bremer, D. Y. Chen, A. Malko, M. Madel, N. Rorsman, S. E. Gunnarsson, K. Andersson and M. Thorsell, "Thermal Characterization of GaN HEMTs Affected by Trapping Effects Using Electrical Measurements," submitted to *IEEE Transactions on Electron Devices*, 2019.

[B] J. Bremer, J. Bergsten, L. Hanning, T. Nilsson, N. Rorsman, S. Gustafsson A. M. Eriksson and M. Thorsell, "Analysis of Lateral Thermal Coupling for GaN MMIC Technologies," *IEEE Transactions on Microwave Theory and Techniques*, vol. 66, no. 10, pp. 4430-4438, October, 2018.

[C] J. Bremer, L. Hanning, N. Rorsman and M. Thorsell, "Compensation of Performance Degradation Due to Thermal Effects in GaN LNA Using Dynamic Bias," in *48th European Microwave Conference*, Madrid, September, 2018, pp. 1213-1216.

Other Publications

The content of the following publications partially overlaps with the appended papers or is out of the scope of this thesis.

[a] L. Hanning, J. Bremer, M. Ström, N. Billström, T. Eriksson and M. Thorsell, "Optimizing the Signal-to-Noise and Distortion Ratio of a GaN LNA using Dynamic Bias," in *91st ARFTG Microwave Measurement Conference*, Philadelphia, PA, June, 2018, pp. 1-4.

[b] J. Bremer, N. Rorsman and M. Thorsell, "A Novel Test Structure for Electrothermal Assessment of GaN Technologies," in *9th Wide Bandgap Semiconductors and Components Workshop*, Harwell, October, 2018, pp. 1-5.

Contents

Chapter 1

Introduction

Wide bandgap semiconductors, in particular gallium nitride (GaN), have emerged as viable materials for fabrication of transistors with high power density and breakdown voltage. This has made GaN technology an important tool in the work to meet the performance requirements in areas such as the defence, wireless communication, and power electronics industries. Power transistors need to withstand high voltages and minimize resistive losses to meet efficiency and voltage conversion demands. The mobile phone networks primarily see increased demands on higher user data rate, improved energy efficiency, and lower cost. From 2018 to 2019, 530 million new subscriptions were made globally to mobile broadband services, and the total mobile data traffic during 2019 was 38 exabytes per month [1].

To cope with these demands, microwave electronics, with higher output power, higher efficiency, and lower noise continuously has to be developed. Larger bandwidth is required to accommodate the increased data rate and therefore transistors need to be able to operate at higher frequencies. In the 5th generation of wireless communication systems (5G), operating frequencies up to 60 GHz are expected and wireless links in future backhaul networks are discussed to operate at frequencies up to 170 GHz [2]. For radar applications, the output power as well as the sensitivity and robustness of the receiver are of concern. The RF output power has to be maximized to increase the range and the receiver must be sensitive to detect objects with small radar cross sections. The transmit-receiver module must also be able to withstand large input signals without losing any sense/detection capabilities.

GaN based high electron mobility transistors (HEMTs) exhibit great characteristics for the above requirements. The performance is enabled by the large bandgap of GaN (3.4 eV), its large electron velocity (2×10^7 cm/s), together with the ability to form HEMT epi-structures with high electron mobility ($> 2000\,\mathrm{cm}^2/\mathrm{Vs}$) and large electron sheet density ($> 1 \times 10^{13}\,\mathrm{cm}^2$). The large and direct band gap structure leads to robust devices that can operate at high voltages. The high electron mobility and large sheet density enable high current densities in the transistors. Furthermore, the large electron velocity enables high frequency performance with f_T and f_{max} reaching over 400 GHz [3]. These material properties lead to high output power densities (Pout = 3 W/mm) at operating frequencies up to 100 GHz [4]. In addition, low specific on-resistances ($< 4.5\,\mathrm{m}\Omega\mathrm{cm}^2$) for breakdown voltages up to 2 kV can be achieved [5].

The performance of GaN HEMTs is currently limited by dispersive effects caused by electron trapping and self-heating. Trapping effects are caused

by trapping states located mainly on the surface and in the buffer of the AlGaN/GaN heterostructure. It gives rise to various forms of frequency dispersion e.g. DC-current dispersion, current collapse, and RF-current slump, which lead to reduced output power, efficiency, and premature gain compression [6].

The material properties of GaN allow for 5-10 times higher power densities compared to GaAs [7]. Furthermore, the theoretical limit is beyond 40 W/mm, which has been demonstrated on single finger HEMTs and with short pulses. [8]. Such power levels cannot be used in real applications since the devices would undergo excessive self-heating, which would degrade the performance and risk reducing the mean time to failiure (MTTF). Currently, commercial monolithic microwave integrated circuit (MMIC) foundries are rated in the order of 5 W/mm to keep the channel temperature below 200 °C [7], and thus maintaining a certain minimum MTTF. GaN devices can withstand higher maximum junction temperatures (up to 400 °C). Regardless, the work on increasing the power density of GaN HEMTs is limited by self-heating and the ability to remove the heat caused by the dissipated power in the MMIC.

The thermal limitation can be overcome by either increasing the device efficiency, which reduces the dissipated power, or improving the heat extraction. The latter concerns thermal management, where heat extraction is improved by means of remote or integrated, passive and active cooling. Passive remote cooling is the traditional approach for high power GaN chips, where the die is attached to a heat-spreader and package with thermal interface materials (TIMs). The device temperature is set by the thermal resistances in the GaN-die, heat spreader, TIMs, and package, where the heat spreader should have minimal thermal resistance and a matching coefficient of thermal expansion (CTE). For near-junction cooling, high thermal conductivity substrates such as SiC (500 W/mK) and chemical vapor depositioned diamond (2000 W/mK) have been developed. This type of cooling is mainly limited by the thermal boundary resistance (TBR), which is introduced by the substrate-GaN interface [9].

In addition to the heating, which introduces thermal memory effects, GaN devices are subjected to electrical memory effects caused by the electron trapping. These effects are interacting with each other and must therefore be well understood. Characterization methods need to be developed as well as extended to correctly handle self-heating in order to accurately estimate e.g. the thermal resistance. Furthermore, as the size of circuits decreases at higher frequencies, the laterally coupled heat between devices becomes significant, and is therefore important to measure and understand. Chapter 2 is dedicated to electrical characterization techniques, including measurements of the lateral and vertical heat properties as well as trapping effects.

Increased operating temperature degrades the physical parameters such as electron mobility and saturation velocity, leading to reduced current in the transistor. These thermal effects generally degrades the performance of MMICs in terms of output power, gain, efficiency, and noise [10]. Since these characteristics largely depend on the electrical stimulus, electric-based temperature compensation techniques can also be employed to mitigate thermal performance loss. In chapter 3, a biasing technique to make several performance parameters of a GaN MMIC temperature insensitive is evaluated.

Chapter 2

Electrothermal Characterization

Electrothermal characterization provides information of both the thermal and electrical properties of the device. It is a central part in e.g. the work to optimize the epi-structure and substrate since thermal optimization may have adverse effects on the electrical performance and vice versa. The electrical characteristics are affected by various forms of dispersive effects, which mainly originate from electron trapping and self-heating. Trapping effects modulates the current via the trapping/de-trapping of trapping states. Self-heating affect the current via the temperature dependence of the electron mobility. In general, both these effects degrade the electrical performance and they are coupled to each other via the dissipated power. Thermal effects hence also include how heating influences trapping effects and its impact on the current.

An exemplifying scenario is the load-line for a class-B biased transistor. It passes through regions with high electric fields and varying power dissipation. This causes charging/discharging due to traps in the material as well as variations in device temperature according to e.g. the envelope of modulated signals. As a result, signals applied to the device are distorted accordingly [11]. It is difficult to predict the resulting IV characteristics and non-trivial to separate trapping effects from from self-heating due to the overlap in time constants (100 ns - 100 s) [12]. Paper [A] studies the effects of trapping and self-heating on the current in GaN resistors. Such devices are easily fabricated and general measurement results also apply for HEMTs. Electrical measurements methods are presented and used to identify conditions where self-heating dominates the current behaviour. This enables the extraction of thermal properties from electrical measurements, which is very useful in order to thermally evaluate e.g. packaged devices.

Paper [B] is dedicated to characterization of the lateral heat spread in GaN on silicon carbide (SiC) samples. Significant heat coupling can be exhibited due to thermal barriers and the difference between the in plane and transversal thermal conductivity of the SiC substrate. Time constants and heat propagation characteristics at different operating temperatures are obtained from transient measurements. These are parameters of interest from a circuit simulation and thermal management perspective.

2.1 Current Transport in GaN 2DEG

A GaN heterostructure forms a two dimensional electron gas (2DEG), which constitutes the conductive channel. The current transport in the 2DEG depends on the applied lateral electric field, channel temperature as well as charge in the vicinity of the 2DEG due to e.g. a gate contact or trapped electrons. The electron drift current can be modeled by

$$I_d = qn_s v_d \left(\mu_e \left(E, T_c\right), E\right) W, \tag{2.1}$$

where q is the electron charge, n_s is the electron density in the 2DEG, v_d is the electron drift velocity, μ_e, is the electron mobility, E is the electric field, T_c is the channel temperature and W is the width of the GaN resistor. Under ideal conditions, I_d is set by the isothermal field dependent electron drift velocity $v_d = v_d(\mu_e(E), E)$ [13]. However, self-heating reduces the electron mobility due to e.g. polar optical phonon scattering at higher temperatures [14], which in turn affects the drift velocity [15].

Electron trapping in the buffer and at the surface give rise to a virtual gate effect. The charging and discharging of such traps modulate the vertical electric field and n_s accordingly. The traps may have different activation energies and the trapping of electrons depends strongly on the kinetic carrier energy and hence applied electric field [16, 17]. The de-trapping also depends on the field but is also strongly dependent on T_c and hence on the ambient temperature, T_a, and dissipated power, which is also field dependent. Because of the simultaneous dependence on E of both n_s and v_d, it becomes difficult to isolate the impact of self-heating from a measurement of I_d.

2.1.1 Self-heating versus Electric Field

It is clear that the dispersive effects will manifest differently depending on the voltage sweep and device geometry. For an accurate thermal analysis, the self-heating ($v_d(T_c)$) must be isolated from trapping effects i.e. n_s should ideally be constant and independent of E and T_c. The electric field is reduced either by decreasing the applied voltage or increasing the contact separation. Furthermore, the self-heating needs to be enhanced by increasing the dissipated power, P_{diss}. It is directly proportional to the dissipated power in the resistor, which can be expressed in the linear region as

$$P_{diss} = qn_s \mu_e W \frac{V^2}{L}, \tag{2.2}$$

where V is the voltage and L is the contact separation. Equation (2.2) shows that it is better to reduce the field by increasing the contact separation ($\propto 1/L$) rather than decreasing the voltage ($\propto V^2$) in order to maintain a high joule-heating [18]. In addition, the devices may be scaled up (W) to increase the power. Fig. 2.1 shows the power dissipation and power density versus E for different contact separations. The power dissipation is increasing with contact separation, while the power density is similar or slightly higher (right y-axis) for the longer resistors. This results in higher self-heating (and channel temperature). Consequently, the resistance increase versus field is larger for longer contact separations as is indicated by the larger reduction of the current derivative for the longer resistors in Fig. 2.1(inset).

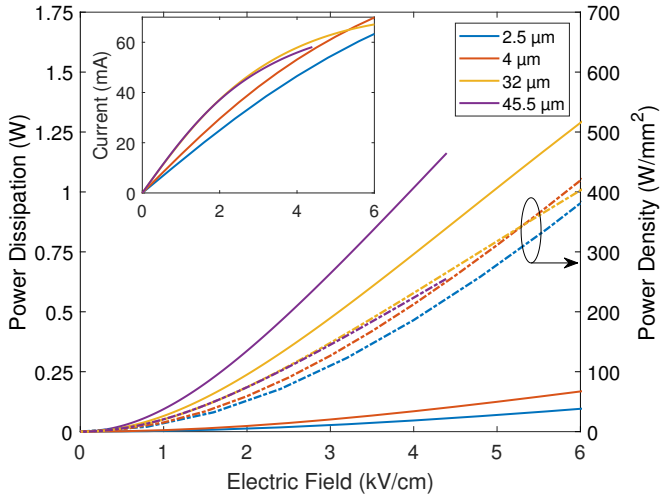

Figure 2.1: Power dissipation/density (main figure) and current (inset) versus electric field of four GaN resistors with different contact separation.

2.1.2 Temperature Dependent IV

A simple way to evaluate (2.1) with a well defined homogeneous field is to remove the gate and only control the lateral field of the resulting GaN resistor. This makes it easy to see trapping-originating effects on n_s and it also simplifies the measurement methods by removing the second port. One disadvantage is not to be able to turn off the channel while applying high fields (pinch-off measurements). Fig. 2.2 shows GaN resistors configured as transfer length method (TLM) structures with 100 µm width, and contact separations 3-50 µm. In paper [A], experiments were carried out on for different samples, M1-M4, which have varying parameters that are of importance for thermal properties (section 2.2.3).

The current characteristics depend on the trapping characteristics that affect I_d via n_s. This depends on the available trapping states (activation energy and density), which is determined by the epitaxial design and fabrication of the heterostructure. Consequently, the IV versus temperature characteristics may behave very differently between different samples. Normally, the current is expected to decrease for higher temperatures. However, if $\mu_e(T_c)$ is not the

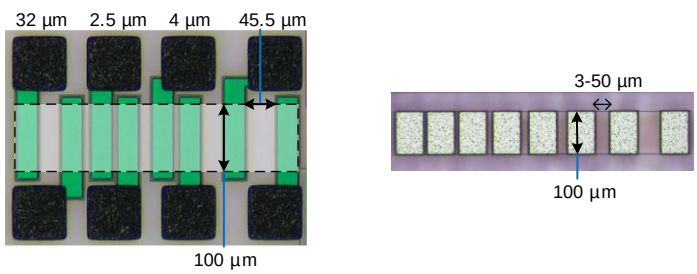

Figure 2.2: Chip photographs of GaN resistors configured as TLM structures.

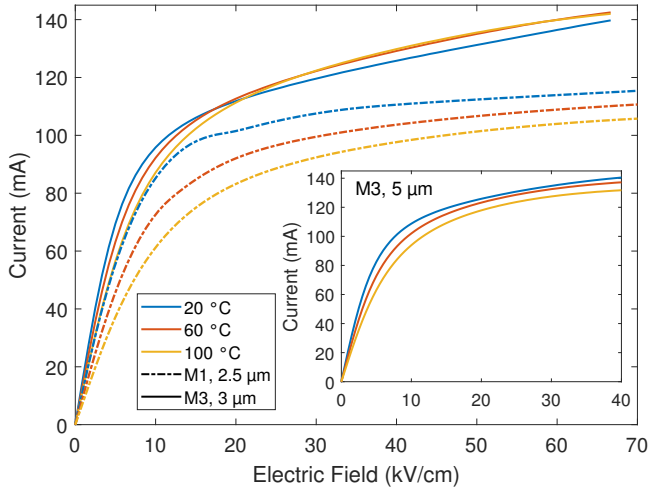

Figure 2.3: Current versus electric field of GaN resistors on two different samples. Main figure: A 2.5 µm (sample M1) and 3 µm (sample M3) contact separated resistor. Inset: A 5 µm long resistor (sample M3).

dominant temperature-dependent factor, this may not be the case. The current versus average electric field of the 2.5 µm (M1) and 3 µm (M3) resistors is shown in Fig. 2.3(main). For M3, the current is first decreasing with temperature up to 15 kV/cm, after which the temperature dependence is inverted due to the trapping characteristics. The channel temperature increases with E and a positive current-temperature coefficient suggest n_s is increasing more than μ_e is decreasing as T_c rises. In contrast to M3, a negative current-temperature coefficient can be seen for M1 (dashed line) throughout the whole measurement. However, a kink-effect [19] can be observed around 20 kV/cm at 20 °C, which shows that M1 is not trap free.

The positive current temperature coefficient above 20 kV/cm for the 3 µm resistor of M3 does not appear for the 5 µm resistor, as seen in the inset of Fig. 2.3. A larger contact separation is therefore beneficial to avoid high fields and trapping of electrons. This is useful in order to study self-heating effects more separately.

2.1.3 Differential Resistance Measurements

The extent to which trapping and self-heating individually affect the current is not obvious for devices with longer contact separation, and for samples with less trapping (M1 Fig. 2.3). In such cases, further information can be gained by studying the differential resistance $r = (\partial I_d(V, T_a)/\partial V)^{-1}$. When only considering the mobility-temperature dependence, r is expected to increase as T_a increases. A decreasing $r(T_a)$ characteristic is therefore an indication of electron trapping.

In paper [A], differential resistance characteristics were investigated for both long and short contact separations, as shown in Fig. 2.4. In general, it can be seen that there is a region at low fields, which exhibits a positive temperature coefficient ($\mu_e(T_c)$ dominates), and a region at higher fields where this is no

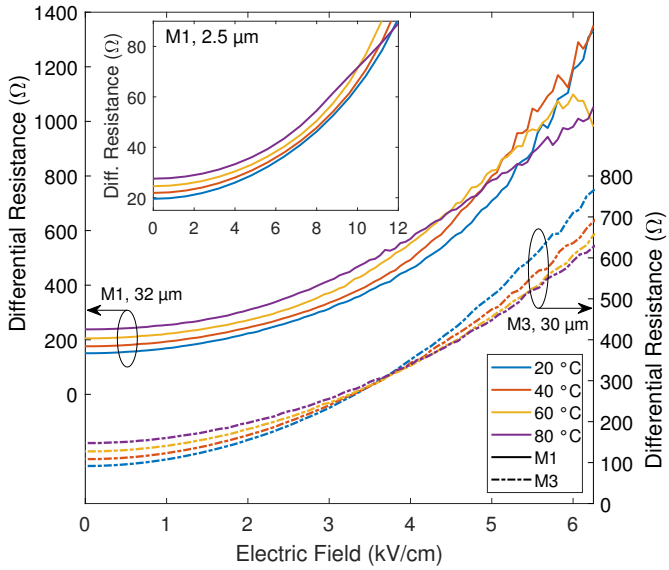

Figure 2.4: Differential resistance versus electric field of GaN resistors on two different samples. Main figure: A 32 µm (sample M1, solid line) and 30 µm (sample M3, dashed line) contact separated resistor. Inset: A 2.5 µm long resistor (sample M1).

longer the case. As an example, the 30 µm resistor (M3) exhibits a positive temperature coefficient up to approximately 3 kV/cm (Fig. 2.4(right y-axis)). Above 5 kV/cm, a negative temperature coefficient can be seen, indicating an increasing n_s as T_c rises. In addition, it can be observed that M1 has a larger region with a positive temperature coefficient compared to M3.

The differential resistance measurement offers a simple tool identify the onset of significant trapping effects. It is also a practical tool to quantify the amount of self-heating in terms of resistance increase, as discussed in paper [A].

Low Field Dispersive Effects

Although self-heating is dominating at low fields, it is still of interest to know how electron trapping affect the low field characteristics. As was seen in section 2.1.2, the trap dynamics are strongly temperature dependent, and hence the resistors could exhibit de-trapping effects at low fields (0-3 kV/cm) if T_a is high enough. The low field resistance for each resistor is given by

$$R_{meas} = 2\frac{R_c}{W} + R_{sh}\frac{L}{W}, \tag{2.3}$$

where, R_c is the contact resistance, R_{sh} is the sheet resistivity and R_{meas} is the measured DC resistance, which is equal to r at low fields. $R_{sh} = 1/qn_s\mu_e$ is a geometry independent material parameter that is expected to be approximately the same for all resistors. Fig. 2.5 shows the extracted R_{sh} of different GaN resistors from a TLM structure. The shorter contact separations can be seen to have a significantly higher sheet resistivity due to the electron trapping caused by the higher electric field. The 32 µm and 45.5 µm resistors yield a similar resistivity, as expected due to the large contact separation. It is possible that

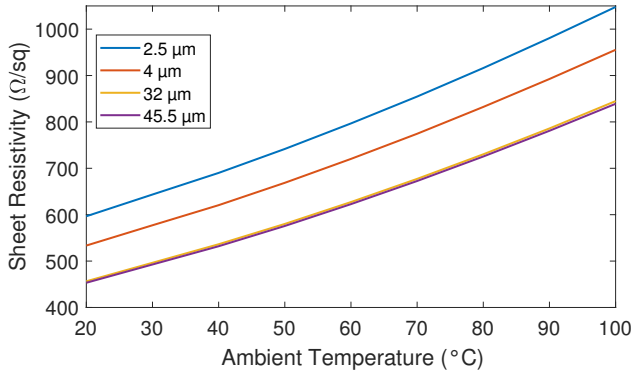

Figure 2.5: Extracted sheet resistivity versus ambient temperature of GaN resistors with different contact separation.

the observed impact on the sheet resistivity, which remains up to 100 °C are due to deep level trap states.

In general, the critical combination of T_a and the electric field can be seen by studying $r(T_a)$ and $dr(T_a)/dT_a$ at lower fields around 0.5-3 kV/cm, as performed in paper [A]. Such measurements provide a detailed overview and indicate at what voltage and ambient temperature that the thermal analysis should be performed.

2.2 Temperature Measurements

Numerous techniques for measuring the channel temperature and associated thermal resistance of microwave devices exist. The methods may be initially divided in three categories: electrical, physical, and thermal imaging, where the methods are either of steady-state or transient analysis type. A brief review and discussion of these methods is presented here followed by the methodology presented in paper [A].

2.2.1 Optical Methods

Thermal characterization of GaN has some unique challenges compared to Si and GaAs. The wide bandgap leads to transparency and thin film interference issues, which can lead to errors for thermal imaging techniques such as infrared radiation (IR) imaging, thermoreflectance (TR) thermal imaging, and Micro-Raman spectroscopy. Nevertheless, the majority of temperature measurements of GaN devices is carried out using these methods. Raman and TR partly overcome some of the challenges but are associated with their respective limitations. Advantages with optical measurements include a direct measurement of the channel temperature (steady state or transient) with high resolution, without the need to modify or physically contacting the DUT. Optical access to the device is however required, which cannot be provided for packaged devices. Detailed studies on GaN HEMTs using these methods can be found in [20–22]. In the following sections, each method, along with its associated advantages/disadvantages, is briefly presented and discussed.

Infrared Radiation

IR thermography is based on acquiring the intensity of the thermal radiation, which is described by Planck's formula. Real bodies do not exhibit perfect absorption and emission and the frequency-dependent emissivity (ε) of the object (grey body) has to be taken into consideration. The total energy flux is given by Stefan–Boltzmann law, $P = \varepsilon\sigma AT^4$, however, a sensor only measures a limited part of the spectrum.

The energy impinging on a material must either pass through, be absorbed, or be reflected (transmissivity, absorbtivity, and reflectivity), and the sum of these three properties must add to unity. Good absorbers are equally good emitters (emissivity = absorbtivity). In this case, all emitted light originates from thermal radiation and the temperature accuracy can approach mK. Metals tend to be very reflective and may have emissivity $\varepsilon < 0.1$. In this case, a large part of the measured signal originates from reflected light, and the instrument mostly measures the ambient temperature or system noise level. The emissivity of semiconductors can vary in the range between 0.3 and 0.8. Undoped silicon is transmissive for infrared wavelengths > 1.1 µm but doped silicon is absorptive (and emissive). Plastics, ceramics, glue, and many organics are very absorptive.

In IR thermography, the signal is collected by an optical system, consisting of a microscope, IR optics, and an IR sensitive detector array. The varying emissivity of different parts of the circuit is compensated for with a correction algorithm. By measuring the IR intensity from the circuit at a known temperature, the emissivity at each pixel can be obtained, which can then be used to compute the temperature of the powered device.

To obtain the temperature of low-emissivity materials, the temperature of such materials has to be raised substantially above the background temperature. High-power devices may quickly degrade and fail at these temperatures, making the measurement difficult to perform. Absolute temperature uncertainty increases with temperature and can reach 20–50 °C for a temperatures higher than 400 °C [22]. For wide bandgap semiconductors, which are very transparent for IR wavelengths, considerable depth averaging as well as lateral averaging (due to limited spatial resolution) occurs. In this case, IR emission from deep below the surface reaches the IR detector, and gold metallization on the back contact can reflect more radiation, leading to errors between the calibration and measurement. Consequently, it becomes difficult to determine which temperature is represented by IR thermography. Coating the device with nontransparent material improves the accuracy, however, this method risks causing surface contamination/damage and does not guarantee a correct temperature observation.

IR imaging is beneficial to measure the surface temperature over large areas and is de facto industry standard for channel temperature measurements. It provides a full field temperature mapping with good spatial (1.9 µm) and temporal (3 µs) resolution.

Raman Spectroscopy

Temperature measurements using Raman spectroscopy utilizes the dependence on temperature of the phonon frequency (oscillations of atoms in the crystal lattice). Inelastic light scattering in a material results in a change in the wavelength of laser light incident on the surface due to optical phonon emission. Because of the temperature dependence of the phonon frequencies, Raman spectroscopy can be used to determine the temperature of a localized region if the frequency shift with temperature is obtained from calibration. Materials may exhibit several specific vibrational modes, which can be used to determine temperature, stress/strain, crystal quality and impurities/defects. The GaN Raman spectrum exhibits one strong phonon mode (E2 high) around $568\,\mathrm{cm}^{-1}$ and a weaker (A1 LO) around $735\,\mathrm{cm}^{-1}$. The E2-type phonon mode of the SiC substrate is visible at $778\,\mathrm{cm}^{-1}$. Contact metals do not exhibit easily accessible lines in their Raman spectrum for temperature measurements.

For GaN, the phonon frequency shift can be affected by piezoelectric strain caused by an applied electric field as well as due to the CTE mismatch between the epilayer and substrate. The total change in phonon energy from a change in temperature can therefore be separated into two parts, related to the change in lattice temperature in a bulk strain free material $\Delta\omega T$, and the additional change induced by mechanical strain $\Delta\omega\varepsilon$, including the CTE. A pinch-off measurement can be performed to allow self-heating to be determined separately from piezoelectric strain. The accuracy of Raman measurements depends on the smallest value of frequency change of a given phonon mode, which can be reliably determined from the spectrum. A temperature accuracy around 4 % of the temperature rise can typically be achieved, and the accuracy increases inherently at higher temperatures. The linewidth of the Raman peak also defines the resolution. For SiC, it results in a resolution roughly 2–3 times better compared to GaN, because of the narrower Raman modes.

The method involves focusing a laser onto a sample with an objective lens and passing the scattered light through a Rayleigh filter and onto a spectrograph. After the phonon frequency shift as a function of temperature is obtained for the material, the temperature rise due to self-heating of the device can be extracted by measuring the difference between the phonon frequency of the powered and the unbiased device. Normally, calibration coefficients of both the high and low modes are obtained and both modes are measured at pinch off and at powered conditions. The results are then compared to separate the stress and temperature. It may be needed to measure the relative intensity of the Stokes (phonon creation) and Antistokes (phonon annihilation) processes, which is an alternative method to derive the temperature. Stokes modes appears symmetrically relative to the laser frequency. Theoretically, the ratio of these intensities is material independent.

The Raman method is limited to device areas where the semiconductor material is visible (no top metals) and cannot measure HEMTs with field plates. It can measure the temperature a few microns below the semiconductor surface with high spatial resolution (approximately $0.4\,\mu\mathrm{m}$ laser spot size). With less lateral averaging (compared to IR), it is considered suitable for precise single point channel temperature measurements for HEMTs.

Thermoreflectance

The thermoreflectance measurement technique exploits the temperature dependence of a material's reflectivity. As the temperature of the sample changes, the refractive index, and therefore, the reflectivity also changes. A first order approximation of the reflectivity-temperature relationship is

$$\frac{\Delta R}{R} = \left(\frac{1}{R}\frac{\partial R}{\partial T}\right)\Delta T \equiv C_{th}\Delta T. \tag{2.4}$$

The intensity of the optical reflection of an illumination ($\Delta R/R$) changes with a change in surface temperature (ΔT) and can be related by the thermoreflectance coefficient, C_{th}. The amount that the reflectivity changes with temperature (C_{th}) is a function of the illumination wavelength, the ambient temperature, the material, surface characteristics, and material processing technique. Dielectric coatings and passivation layers change the reflective properties and hence C_{th} must be measured for each surface. C_{th} can be considered to be constant over a wide temperature range however ideally it is measured at the operating temperature of interest. For most metals and semiconductors the value is of the order 10^{-2} /K to 10^{-5} /K. Since it is very small, a lock-in technique is used to enhance the signal to noise ratio (SNR). To achieve the best temperature resolution, the illumination wavelength that maximizes C_{th} for the material should be selected. A trade-off with spatial resolution (wavelength dependent) is therefore sometimes warranted.

A pixel-by-pixel calibration of the TR coefficients allows the temperature information at targeted locations to be derived from the light intensity. Images are detected by either a PIN diode array camera or a special high frame rate intensified charge coupled device (CCD) [23]. TR uses probing light sources in the visible range to achieve sub-micron spatial resolution. The shorter illumination wavelength improves the spatial resolution of the thermal image considerably compared to other techniques. A spatial resolution of 0.25 µm with a diffraction limit at 0.2-0.3 µm for wavelengths 365-780 nm can be achieved. The systems also offer high temporal (0.8 ns) and temperature ($<$ 0.5 °C) resolution. For CCD based thermoreflectance systems, the temperature resolution is generally limited by the quantization threshold of the camera [23]. In general, UV and visible wavelengths (365 nm to 760 nm) results in a diffraction limited spatial resolution. By using UV light $<$ 370 nm, the transmission through the GaN and SiC, which can cause thin-film interference effects that convolute the thermoreflectance signal, is reduced. At 365 nm a clear reflection of the top surface for GaN on SiC is achieved [24].

TR is useful to measure temperature gradients on surface microscopic regions with dimensions smaller than the diffraction limit of IR. It excels at fast transient measurements as well as measuring the surface temperature of semiconductors and metals with high temporal and spatial resolution. TR does not require specific sample heating and can be done at room temperature or even at cryogenic temperatures.

2.2.2 Electrical and Physical Methods

Physical contact methods measure the temperature of an object or material that is making thermal contact to the DUT. Several such techniques exist [25], most of which are not widely used for temperature measurements of GaN devices. This thesis focuses on thermal sensors, such as μRTDs [26], which are integrated in the vicinity or even into the active device. This technique requires no optical access and is useful for e.g. temperature monitoring of circuits. Different types of thermometers have therefore been thoroughly studied for microwave transistors. State of the art implementations can be found in e.g. [27], where a resistive nickel temperature sensor was integrated next to the gate on the drain side of an RF HEMT. In general, the challenges are to accurately measure the channel temperature of the active (measured) device without affecting its performance, as is discussed in section 2.3.1.

Electrical methods make use of temperature dependent parameters such as the drain current [28, 29], gate resistance [30], and Schottky diode current [31] to determine the channel temperature. Normally, the thermal resistance (R_{th}) is determined, which can then be used to calculate the channel temperature for steady state conditions, given the dissipated power. To determine the thermal impedance, AC signal excitations can be combined with gate resistance thermometry (GRT) techniques such as in [32]. In general, the advantage with electrical methods is the capability of a fast initial thermal evaluation without the need for dedicated equipment, as well as to be able to evaluate packaged devices for improved cooling. Some disadvantages is the averaging of the extracted channel temperature, and the sometimes needed modifications to the DUT, which could risk the high frequency performance.

The electrical methods exploit the self-heating in the device and how it affects electrical properties to derive information of the thermal properties. For GaN devices however, section 2.1 shows that dispersive trapping effects also affect the electrical parameters and thus have to be considered. In this situation, techniques using GRT are advantageous since the gate resistance is not affected by trapping effects. Recent work with this technique include frequency-resolved GRT with sub-100 ns time resolution [33].

Pulsed IV Techniques

One common approach is to utilize pulsed IV measurements for thermal characterization as outlined in [28, 29]. In such measurements, the influence of self-heating on the device IV characteristics is studied using different pulse widths and/or pulse periods. The technique relies on the temperature dependence of the on-resistance, R_{on}, as defined in Fig. 2.6. First, a look-up table of R_{on} versus temperature is made by sweeping the ambient temperature using e.g. a thermal chuck. It is assumed that due to the low power dissipation in the R_{on}-region, the ambient temperature equals the channel temperature. In the next step, R_{on} is extracted at a fixed ambient temperature while the device is pulsed from different quiescent bias points, corresponding to different dissipated powers (P_{diss}), as shown in Fig. 2.6.

By mapping the R_{on} versus P_{diss} to the R_{on} versus $T_a = T_c$ look-up table previously created, the thermal resistance can be extracted from the slope of the resulting T_c versus P_{diss} curve. As discussed in [29], the method is highly

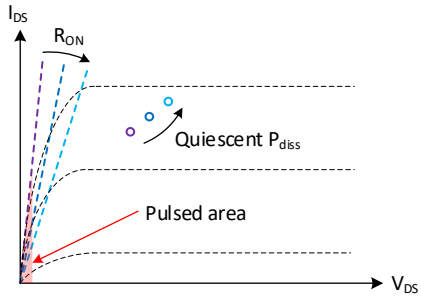

Figure 2.6: Pulsed measurement of the on-resistance from different points of quiescent power dissipation.

dependent on the sub-microsecond pulses to limit cool-down of the device during the R_{on} versus P_{diss} measurement. This can be difficult to achieve since the current starts to decrease even between 3-20 ns [15] for higher levels of power dissipation.

When applying this technique on GaN devices, the impact of trapping effects is typically addressed by stressing the HEMTs with different fields to vary the effect of current collapse. In [29], the stressed and fresh HEMTs yield similar results, which is attributed to the minimal impact of current collapse compared to self-heating in the linear region. These conclusions are however device-dependent and the measurement settings possibly need to be adjusted for more trapping-impacted DUTs.

3ω Methods

The 3ω method [34] is a well established method for measuring the thermal conductivity of dielectric solids. A metal film is deposited on top of a sample, whose thermal conductivity is to be determined. The method uses the radial flow of heat from the metal film, which is used both as a heater and thermometer. The temperature oscillations in the line can be analytically solved for to derive an expression between the slope of the in-phase temperature oscillations versus frequency, and the thermal conductivity.

Next, the temperature oscillations of the metal line are measured by using the third harmonic of the voltage across the line. A current at the angular frequency ω heats the sample as 2ω and produces a temperature oscillation at 2ω. The resistance of the metal increases with increasing temperature and the resistance of the metal line therefore exhibits a small AC component at 2ω. The resistance oscillation (2ω) times the original driving current (ω) produces a small oscillation of the voltage across the line at 3ω. This AC voltage is measured using lock-in amplifiers and is then used to calculate the thermal conductivity. In the derivation in [34], it is assumed that the TBR between the metal line and sample can be ignored. For GaN heterostructures, this is not true due to e.g. the TBR contribution created by the nucleation layer [9].

The key to avoid the impact of trapping effects is to avoid high electric fields. Methods that utilize small AC signals to determine thermal properties are therefore beneficial since high fields are avoided altogether. Therefore, methods similar (e.g. GRT [33]) and methods based on 3ω have been developed

to measure the thermal resistance of GaN HEMTs. In [35], the 3ω method is extended by operating the HEMT in the linear region, and using the channel resistance as a thermometer. In this case, the DUT is placed in a Wheatstone bridge to be able to detect the 3ω signal, which is roughly 90 dB lower than the fundamental. The 3^{rd} harmonic voltage can be expressed in terms of $R_{on}(t)$, the bridge elements and excitation voltages/currents. Consequently, an analytic expression of Z_{th} can be derived because of the $R_{on}(P_{diss}(t), Z_{th})$ dependence. The limitations with this technique are discussed in [36] and involve the parasitic contributions as well as the temperature coefficients (ideally zero) of the bridge components. Also, the requirement of a dedicated test structure itself is practically disadvantageous. An additional inconvenience with this and similar GRT methods is the requirement of high performance signal generators and lock in amplifiers.

2.2.3 Thermal Resistance Extraction

Several of the existing electrical methods require either special test configurations of the DUT, and/or requires dedicated non-standard measurement equipment. The pulsed methods are applicable to most devices but suffer from insufficiently fast pulses. In paper [A], the thermal resistance was extracted using the electrical method in [37], where the thermal resistance is determined at discrete bias points. The method therefore works in good conjunction with the electrothermal characterization in section 2.1, where the measurement ranges first can be established. Because the method uses discrete bias point analysis, R_{th} is provided at different points of quiescent power dissipation. This is a considerable benefit to the afore-mentioned methods, which do not provide any information of the generally nonlinear $R_{th}(P_{diss})$ characteristics. The derivation is described comprehensively in [37] and qualitatively here for the specific devices. It starts with the linear thermal system model

$$T_c(t) = p(t) * h_{th}(t) + T_a, \tag{2.5}$$

where $p(t)$ is the instantaneous power dissipation and $h_{th}(t)$ is the thermal impulse response. The system to solve consist of (2.5) and the general electrothermal device function, $f(i(t), v(t), T_c(t))$. In [37], the electrothermal system is analyzed using a small signal approximation around an equilibrium bias point, to form expressions of the admittance parameters of the device as a function of the thermal transfer function and thermal (current) coefficient. For the 1-port GaN resistors in this work, the extrinsic input admittance is

$$Y_{in}^{ext} = \frac{Y_{in}^{int} + H_{th}(\omega) I_Q \alpha}{1 - H_{th}(\omega) V_Q \alpha}, \tag{2.6}$$

where $H_{th}(\omega)$, is the thermal transfer function α is the thermal coefficient and V_Q, I_Q is the bias voltage and current. Y_{in}^{ext} and Y_{in}^{int} are the input admittance parameters with and without the influence of self-heating, respectively. For static voltages and currents, the temperature coefficient can be shown to be

$$\alpha = \frac{dI/dT_a}{R_{th} V_Q dI/dT_a + 1}, \tag{2.7}$$

where dI/dT_a is the current derivative with respect to ambient temperature. Equation (2.6) and (2.7) can be solved for R_{th} at steady state conditions when $H_{th}(0) = R_{th}$. The solution is

$$R_{th} = \frac{Y_{in}^{ext} - Y_{in}^{int}}{dI/dT_a(I_Q + V_Q Y_{in}^{int})}. \tag{2.8}$$

It can be seen that the thermal resistance reduces to zero when no self-heating occurs ($Y_{in}^{ext} = Y_{in}^{int}$), as expected. Since $Y_{in}^{ext} = dI(V_Q)/dV$ all parameters except Y_{in}^{int} on the right-hand side in (2.8) can be determined with DC measurements at different ambient temperatures. It is therefore beneficial to extract a DC model describing the measurement data to reduce the impact of measurement noise (see paper [A]).

To determine Y_{in}^{int} an isothermal measurement needs to be performed similar to the sub-µs pulses for the pulsed IV method. It can be seen in (2.6) that $Y_{in}^{ext} = Y_{in}^{int}$ when $H_{th} = 0$ i.e. when no self-heating occurs. Thus Y_{in}^{int} can be determined with S-parameter measurements above the thermal response, which are performed at the bias points of interest. Fig. 2.7 shows the input impedance (Z_{in}) obtained from low frequency S-parameters from 5 Hz to 3 GHz. The self-heating increases the resistance significantly at low frequencies with more pronounced impact at 4-8 V due to the higher power dissipation. The cut-off point, where $H_{th}(\omega) = 0$, is approximately at 100 MHz and higher frequency characteristics depend largely on pad parasitics. One advantage with this isothermal measurement is that S-parameter measurements are trivial to carry out with any VNA. There is effectively no upper limitation of how fast signals that can be used. The method also provides a good overview of the parasitic contribution to the result. If needed the parasitics can be de-embedded, provided a sufficient model is available.

An example of the thermal resistance obtained from using equation (2.8) can be seen in Fig. 2.8. In this case, the measurements were performed on

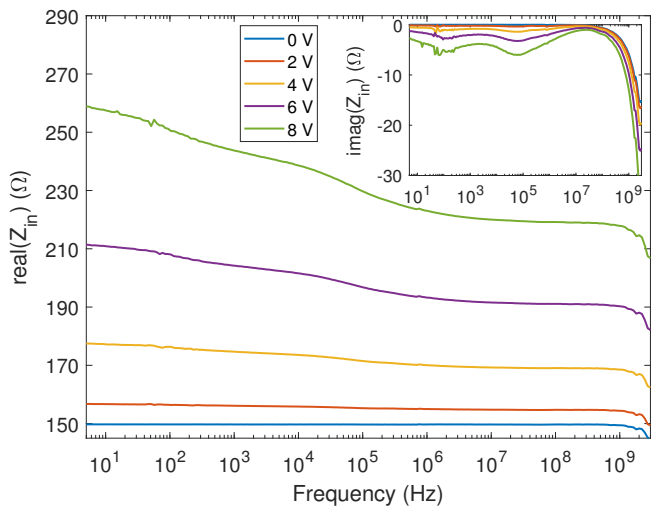

Figure 2.7: Real (main figure) and imaginary (inset) part of the input impedance versus frequency for a 32 µm GaN resistor biased at 0-8 V.

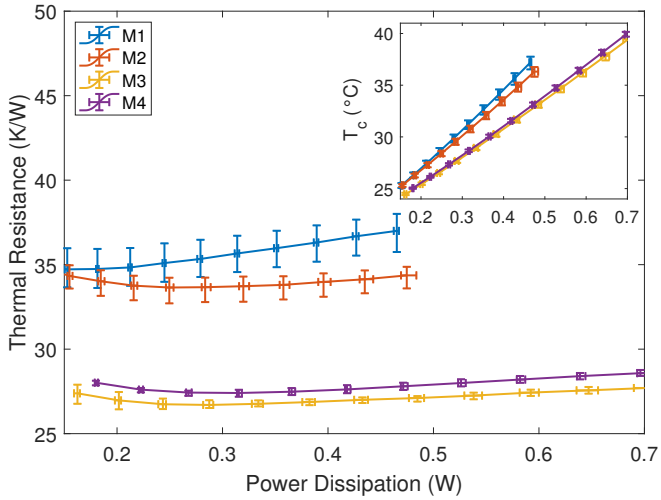

Figure 2.8: Thermal resistance (main figure) and calculated channel temperature (inset) versus power dissipation, for GaN resistors on different samples held at 20 °C ambient temperature. The solid lines are the average value of three resistors and the errorbars show the maximum and minimum values.

resistors with around 30 µm contact separation between 4-10 V at 20 °C, in accordance with prior differential resistance measurements. Three resistors at different locations on the samples were measured and averaged. At low power (4-6 V), the uncertainty is large (insufficient self-heating), which explains the initially decreasing thermal resistance. At higher power (7-9 V), the thermal resistance is approximately constant or increases slowly with increasing power (M1).

M1-M2 have a 100 µm SiC substrate from two different suppliers. A maximum difference of 3 K/W can be seen, which could originate from differences in the crystal quality of the substrates. These samples are on 4" wafers and the measurement positions are far apart. The variation of the thermal resistance could therefore be partly due to non-uniform contact with the chuck.

The M3-M4 samples have a 500 µm SiC substrate, with a thin and thick buffer. In this case, since the substrate supplier is also different, the limited improvement could be due to either the buffer or substrate differences. The measurement positions are close together (16x16 mm^2 samples), which results in a similar backside thermal interface and smaller variations of the thermal resistance.

In general, the values are highly affected by the test rig and depend on if the samples are e.g. glued, screwed, or are placed directly on the chuck. Soldering the samples to a baseplate carrier may reduce the thermal resistance up to 40 % [29]. The lower R_{th} of the thicker substrates (M3-M4) is likely due to the partial lateral heat spread that increases the effective area of the heat source to the chuck. However, since M1-M2 have an Au-metalized backside, a direct comparison between the thin and thick substrate samples is not applicable.

2.3 Lateral Thermal Coupling

The combination of high power MMICs designed at high frequencies inherently leads to a high power density, where the area available for heat removal is reduced. Consequently, self-heating is expected to increase but also the coupled heat between active devices becomes significant. In addition, highly integrated active antenna systems are likely to have densely packed high power microwave transceiver front-ends with spacing in the order of half a wavelength. This will increase the electrical and thermal coupling between the different functional blocks, such as power amplifiers (PAs) and low noise amplifiers (LNAs) [38].

The majority of electrothermal GaN studies characterize the self-heating effects and associated R_{th} measurements is primarily a measure of the vertical heat conduction. It is therefore important to develop methods that are able to characterize the lateral thermal coupling in the technology. This facilitates the technology development, circuit design, and would enable a complete thermal model, which can be used to predict the performance of multi-function GaN MMICs. The thermal coupling is characterized by the speed of the heat propagation, and is dependent on the material composition, layer structure, as well as the distance and the operating temperature. The trade-offs for optical methods over large and small areas (section 2.2.1) make electrical methods an attractive alternative. A dedicated test structure and electrical methodology, which can study the lateral coupling over short and long distances is therefore of interest.

2.3.1 Thermal Sensor

To implement the necessary test structure, an on-wafer sensor is needed that can monitor the operating temperature. Ideally, the sensor is compatible with full MMIC processing and can operate without impacting the normal operation of the HEMT (non-invasive). The sensor should be physically small (high spatial resolution) so that it can be placed close to the measured device. For an active sensor, the quiescent power dissipation must be minimized as the generated heat increases chip temperature and introduces measurement errors by influencing the measurement itself. In addition, high temperature sensitivity and temporal resolution are required to detect weak coupling at long distances.

While the physical sensors in e.g. [26, 27] are viable, it is straightforward to exploit the temperature characteristics of the GaN resistor (section 2.1.2) for a sensor application. In this case, the sensing element is the channel in the GaN layer (compared to surface metals in e.g. μRTDs). This makes it suitable to study the thermal coupling between channels of multiple GaN devices. The proposed sensor in [B] is a small 2x15 μm resistor. Fig. 2.9 shows the IV characteristics from -50 °C to 100 °C. A small bias voltage is desirable to avoid trapping (section 2.1) and reduce the quiescent power dissipation. The contact resistance is approximately constant versus temperature [39]. Thus at low fields, the current's temperature dependence is solely due to changes in the resistivity of the 2DEG. The current-temperature sensitivity can however be seen to increase between the linear region and saturation region (inset).

For accurate temperature estimations, the self-heating needs to be low enough so that the ambient temperature sets the channel temperature ($T_c = T_a$).

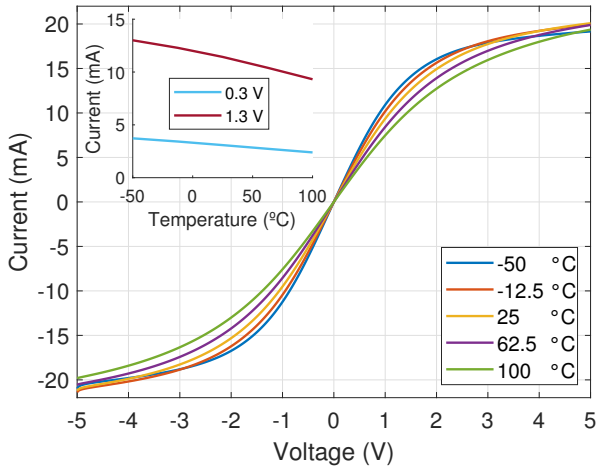

Figure 2.9: IV characteristics of the thermal sensor measured from -50 °C to 100 °C. Inset: $I(T_a)$ characteristics at 0.3 V and 1.3 V.

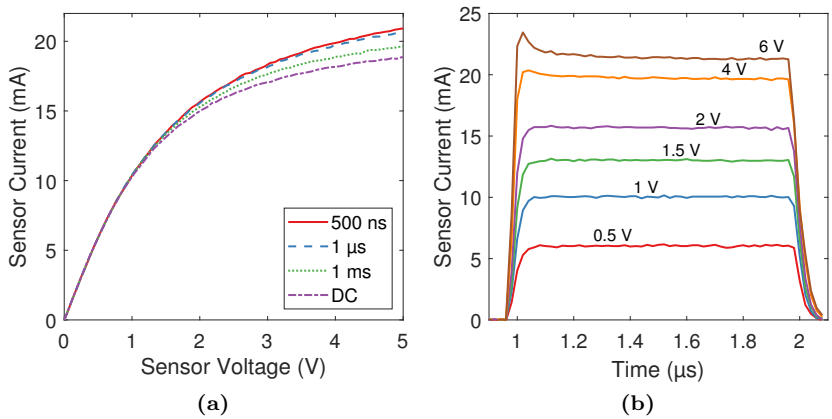

(a) **(b)**

Figure 2.10: Pulsed IV-measurement of the thermal sensor with different pulse widths **(a)** and current time response of the sensor for different voltages **(b)**.

The pulsed IV measurement in Fig. 2.10a shows the impact of self-heating on the sensor IV characteristics. As expected, the self-heating increases as the pulse width increases, in this case from 500 µm to 1 ms. The pulse repetition frequency (PRF) must be low enough to ensure a full recovery of the current. It can be experimentally determined by gradually decreasing the PRF until it does not influence the measurement. As seen in Fig. 2.10a, due to the low power dissipation at low voltages, the effect of self-heating on the current is minimal up to 1.5 V. Hence, bias points up to this level should result in accurate temperature estimations of the sensor. The time domain data in Fig. 2.10b shows that a fast response below 100 ns starts to occur around 4 V. Extremely short pulses are thus needed to see the effect of self-heating at higher voltages.

2.3.2 Thermal Test Structure

A dedicated test area is proposed in [B] that includes both the proposed thermal sensor as well as a heating element to emulate the presence of e.g. a power amplifier. The heating element is a larger, 100 µm wide resistor with 80 µm wide access lines. Fig.2.11(inset) shows the heater with 80 µm access lines to support larger currents. Thermal coupling over both short distances, e.g. between HEMT fingers, and long distances, e.g. between transistor cells, are of interest to study and model. The test structure consists of heaters and sensors with eight different separations, ranging from 86 µm to 484 µm (center to center point). A part of the fabricated test structure can be seen in in Fig. 2.11.

For transient measurements, the idea is to generate a rapid increase in temperature in the heating element by applying a pulsed voltage stimulus. The quick heating will cause a heat propagation in the lateral and vertical dimensions and its propagation properties will depend on the thermal properties of the heterostructure and substrate. Characterization of the lateral thermal coupling is obtained from the transient current response of the sensor, which is located at a known distance from the heater. To perform this measurement, a time domain based measurement system was developed in [B].

2.3.3 Transient Measurements

To evaluate the capabilities of the structure and setup, transient measurements were performed in [B] up to 5 ms. With a sensor biased of 1.3 V, a clear response was observed, enabling detection of power levels of at least 0.5 W. For a series of measurements, the power dissipation in the heater was set fix to 3.1 W. The transient response of the sensor current for all eight separations is shown in Fig. 2.12a. As expected, the magnitude of the response decreases with separation distance, due to the heat spread in all directions (lower half

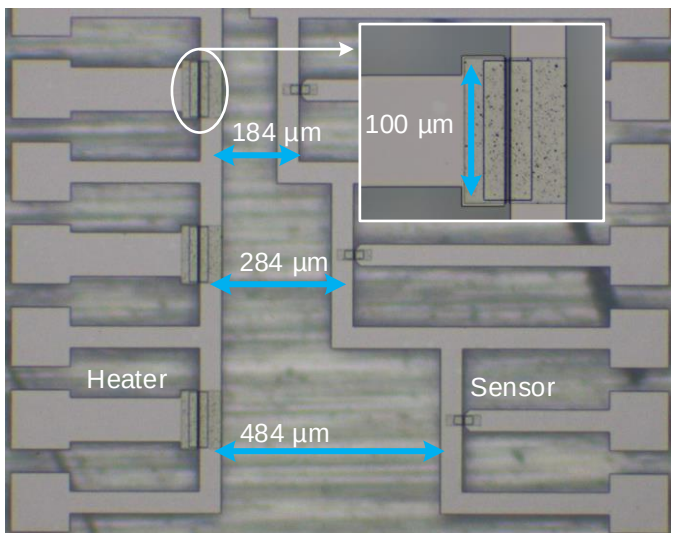

Figure 2.11: Part of test structure for lateral heat coupling measurements consisting of heating elements (left) and thermal sensors (right) with increasing separation distances.

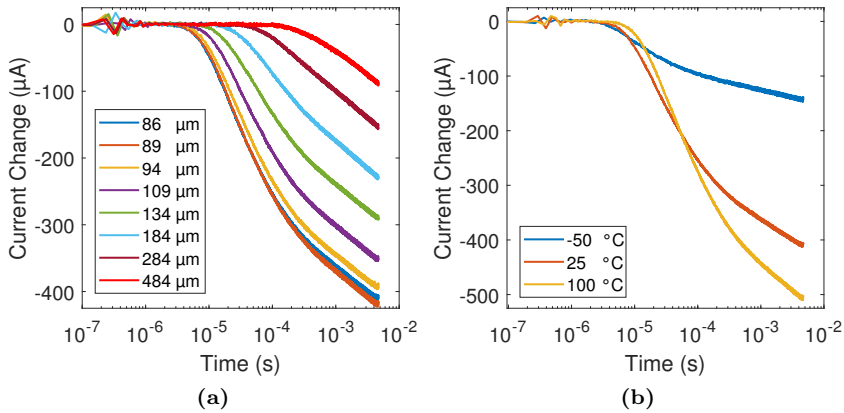

Figure 2.12: Time domain current response of sensors for heater-sensor separations 86-484 μm **(a)**, and current response of a sensor for different ambient temperatures **(b)**.

of a sphere). The shape of the response varies however and a fast transient response is observed within 100 μs for the smaller separations, which becomes less apparent for larger separations. The delay due to the propagation of the heat can be seen to range from approximately 10 μs to 100 μs for the short and long separation distances, respectively. A thermal equilibrium is not reached in the sensor due to the presence of time constants longer than ms. According to theory [40], initially the heat spreads in all 3 dimensions and the heater is similar to a point source in 3D. As the heat reaches the bottom of the substrate, the heat continues to spread mainly in the lateral dimensions due to the lower thermal conductivity of the thermal chuck. As a consequence, the temperature increases logarithmically as from a point source in 2D [40]. The transition crossover between 3D and lateral heat spread can be found from the intersection point between the two different slopes of the response in Fig. 2.12a.

The temperature dependence of the heat coupling is evaluated with measurements at different ambient temperatures, as shown in Fig. 2.12b, where the sensor at 86 μm separation is measured at -50 °C, 25 °C and 100 °C. The propagation delay has a notable temperature dependence and increases several microseconds at 100 °C. At lower temperatures, the magnitude of the response decreases, which indicates a significant temperature dependence of the GaN and SiC layers.

2.3.4 Modeling

The sensor needs to be calibrated to measure the temperature. Fig. 2.9(inset) show that the $I(T_a)$ characteristics are approximately linear in the low voltage (linear IV) region and hence a linear model is generally sufficient. However, as the voltage increases, the IV and $I(T_a)$ characteristics become more nonlinear. To capture and analyse this behaviour, a model of both the voltage and temperature is required. The following empirical electrothermal model is proposed for this purpose

$$I(T_a, V) = (a_1 + a_2 T_a) \tanh(V(b_1 + b_2 T_a)) + V(c_1 + c_2 T_a), \tag{2.9}$$

where V is the voltage and T_a is the ambient temperature. a_{1-2}, b_{1-2} and c_{1-2} are fitting parameters. This expression enables bias voltages up to 2 V to be modelled and is mainly limited by the trapping effects, which are not taken into account. Fig. 2.13(main) shows the model and measurement at 1.3 V, showing a good agreement with the measurement. The insets shows the calculated transient sensor temperature at 86 µm separation at different ambient temperatures. Initially the temperature of the sensor equals the ambient temperature (Fig. 2.13(a)), and it starts to increase as the heat reaches the sensor. The temperature change (Fig. 2.13(b)) indicates a larger thermal coupling at higher ambient temperatures. The reduced thermal coupling at -50 °C compared to 100 °C is likely due to increased thermal diffusivity in the SiC and GaN layers at lower temperatures [41].

By using a model of exponential terms, it is possible to determine the number of thermal time constants present in the transient response. Although strictly empirical, the model provides an analyzing tool to determine e.g. the delay and it is a useful characterization to compare between different heterostructures. In addition, the exponential terms can be used to synthesize thermal circuit models, consisting of R (thermal resistance) and C (heat capacity) circuit elements. The following empirical model is proposed in paper [B]

$$I(t) = I_0 + \sigma(t - t_{del}) \sum_{n=1}^{3} A_n (e^{-(t-t_{del})/\tau_n} - 1), \tag{2.10}$$

where

$$\sigma(t - t_{del}) = \begin{cases} 0, & t - t_{del} < 0 \\ 1, & t - t_{del} \geq 0 \end{cases} . \tag{2.11}$$

The model includes a DC term, I_0, and exponential decay terms, with amplitude coefficients (A_n) and time constants (τ_n). The step function (σ)

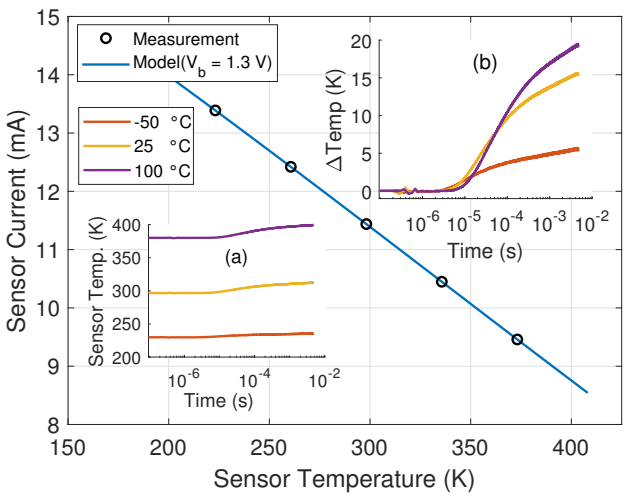

Figure 2.13: Main figure: Measurement (o) and model (-) of a sensor biased at 1.3 V. Insets: transient sensor temperature at different ambient temperatures for a sensor located 86 µm from the heat source.

models the propagation delay (t_{del}). Three terms resulted in a good fit to the measurements in [B], however samples with thinner substrates may require fewer terms [b]. Fig. 2.14 shows the propagation delay ranging between 1-200 µs for the different separations and ambient temperatures. The heat diffuses more slowly at elevated temperatures, as implied by the increased delay at higher ambient temperature.

The significance of each term can be understood by studying the amplitude coefficients. It was found in the study that the coupling mechanism depends on all three time constants for the shorter separations. However, for longer separations, the response contribution of the faster time constants became almost insignificant.

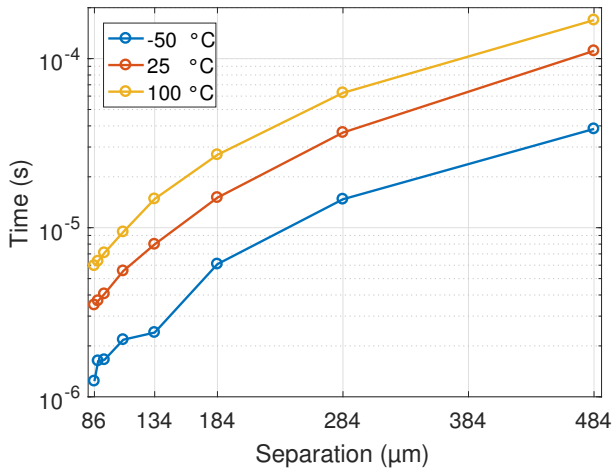

Figure 2.14: Dependence of the propagation delay on the ambient temperature and separation distance.

Chapter 3

Temperature Insensitive MMIC

When the removal of heat is insufficient, the operating temperature of the circuit increases, which results in a general reduction of the circuit performance. At this point, the effects can only be mitigated by either increasing the cooling or compensate for the performance degradation effects with electrical compensation techniques. Solutions regarding the latter exist in the form of analog on-chip compensation circuits and digital off-chip regulators using on-chip sensors. For CMOS RF amplifiers, techniques utilizing analog adaptive bias include zero-temperature coefficient biasing, constant-transconductance biasing, and proportional-to-absolute temperature biasing [42, 43]. In these techniques, the bias circuit is designed to generate a desired voltage/current versus temperature characteristic that, when applied to the biased circuit, counteracts the effects of higher operating temperatures.

For GaAs MMICs, an early proposal for a temperature compensation circuit is [44], which uses a diode and a resistor. It utilizes the temperature characteristics of the diode (decreasing threshold voltage with increased temperature) to increase the gate voltage in the PA and therefore maintaining the gain at higher temperatures. Another topology is demonstrated in [45]. In this case, an active temperature compensation bias circuit is implemented with a current mirror as well as thin film resistors and mesa resistors. With these resistor types, the method can exploit the negative and positive signs of the temperature coefficients of the different resistors to cancel out resistance changes.

Electrical compensation techniques rely on the fact that the transistor properties such as the current exhibit a stronger dependence on electrical stimulus rather than thermal stimulus. It is well known that drain voltage modulation can be used to enhance properties such as linearity and efficiency. Paper [C] evaluates the use of supply modulation to compensate for thermally-induced performance degradation in a GaN LNA. Multi-variable characterization and modeling of several RF parameters is employed to identify trade-offs and limitations which are involved using this technique.

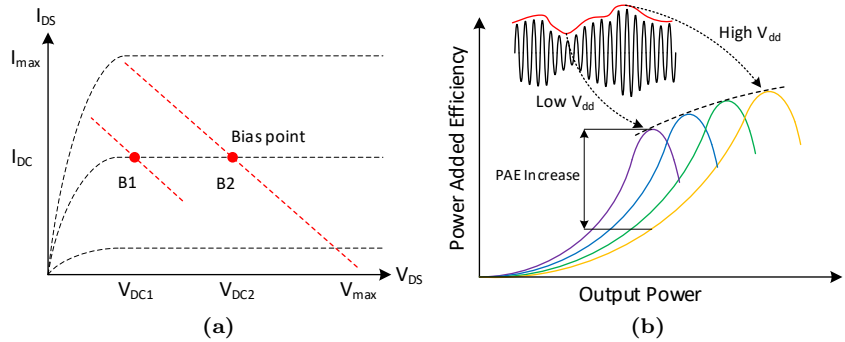

Figure 3.1: Principle of envelope tracking. **(a)** transistor output characteristics with two bias points and RF signals with low (B1) and high (B2) amplitude. **(b)** power added efficiency versus RF output power and different drain voltages.

Envelope Tracking

Supply modulation techniques are traditionally used to enhance the efficiency of the PA in transmitters. PAs are usually biased so that there is sufficient DC power (P_{dc}) at the drain to supply for peak output RF power (P_{out}) conditions. However, when the amplifier is backed-off from peak output power, the excess DC power is dissipated in the transistor since it is not being transformed into RF power.

Envelope Tracking (ET) is an efficiency enhancement method that adjusts the drain voltage to match the needed output power. It can be understood from the bias points in Fig. 3.1a. At maximum output power, the load line at B2 swings from the maximum to minimum voltage and the ratio P_{out}/P_{dc} is as large as it can be for this bias point. If less power is needed from the transistor, corresponding to e.g. the load line at B1, the transistor still has the same DC power consumption. Consequently, more DC power is dissipated as heat, and the power added efficiency (PAE) decreases. This can be avoided by adjusting the bias voltage so that only enough power is supplied to allow for the necessary load line swing, as is the case for the bias point B1 in Fig. 3.1a.

Fig. 3.1b shows the PAE for a PA versus RF output power and different drain voltages. For a constant amplitude signal, the PA is biased to operate at its peak efficiency point. When the signal has a high peak-to-average power ratio (PAPR) and thus varying envelope, as seen in Fig. 3.1b, the PA is occasionally forced to operate with less efficiency if the drain voltage is kept fixed. As can be seen, the peak in efficiency occurs at a lower output powers for lower bias voltages. Envelope tracking allows for the efficiency to track the peaks of the swept bias voltage, resulting in a considerable improvement.

3.1 MMIC Characterization

A commercial 2-6 GHz GaN-on-SiC MMIC LNA, which is suitable for wireless communication and aerospace applications was selected to study in paper [C]. An extensive characterization of the amplifier (Fig. 3.2a) was conducted, including complete RF measurements as functions of gate and drain bias, (V_{gs}, V_{ds}),

as well as ambient temperature. The setup (Fig. 3.2b) performed the measurements by first setting the operating point and then sequentially measuring the gain, output third order intercept point (OIP3), 1 dB compression point (P1dB) and noise figure (NF).

Each operating point is defined as (f, V_{gs}, V_{gs}, T_a), where f is the RF frequency. When the frequency is held fixed, the parameters can be visualized as surfaces plotted against a grid of (V_{gs}, V_{ds}) points. The dependence of the parameters on the bias point can be seen in Fig. 3.3a-d, where the ambient temperature is fixed at 25 °C. It can be concluded that all parameters are fairly sensible to changes in the drain and/or gate voltages. The gain (Fig. 3.3a) exhibits a strong dependence on V_{ds} whereas the OIP3, P1dB and NF (Fig. 3.3b-d) show a strong dependence on V_{gs}. As a reference, the marked red circle in Fig. 3.3a-d shows the recommended bias point.

As the ambient temperature increases, the channel temperature rises and the

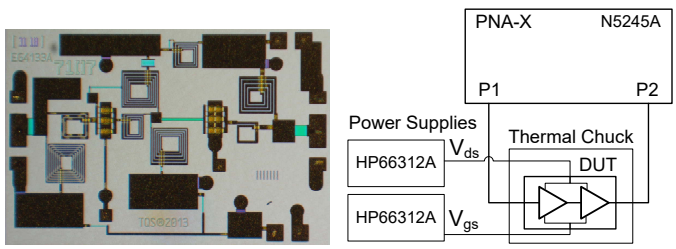

Figure 3.2: Photograph of MMIC low noise amplifier **(a)** and block diagram of measurement setup **(b)**.

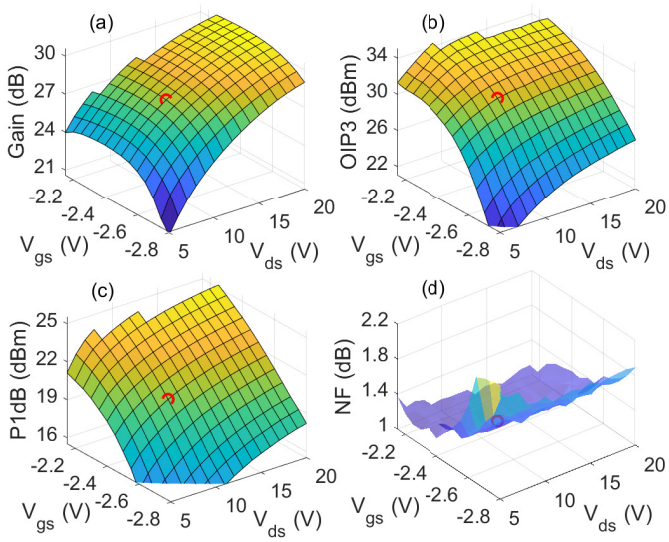

Figure 3.3: RF measurements of GaN LNA for different bias points. The Gain **(a)**, OIP3 **(b)**, P1dB **(c)**, and NF **(d)** are evaluated at 25 °C. The red circle marks the recommended bias point.

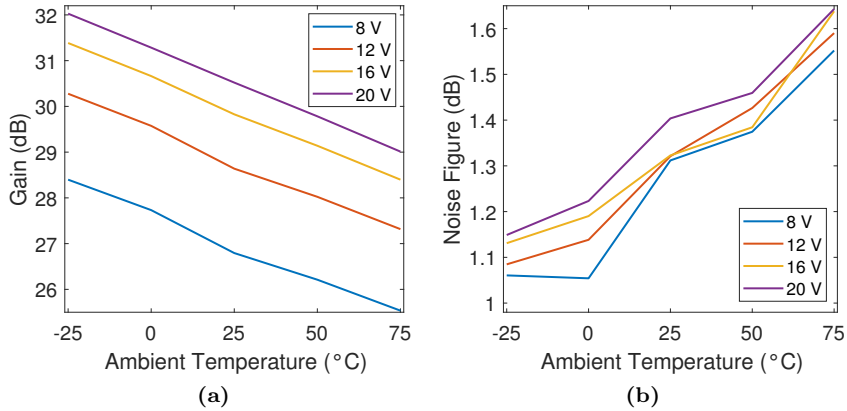

Figure 3.4: Gain **(a)** and noise figure **(b)** of a GaN LNA at different ambient temperatures and for different drain voltages.

noise figure and gain starts to deteriorate, as seen in Fig. 3.4. The gain (Fig. 3.4a) is reduced between 2-3 dB whereas the noise figure (Fig. 3.4b) increases around 0.5 dB within the measured temperature range. The main contributor to the noise increase is thermal noise from different parts in the circuit, whose noise power increases proportionally to its operating temperature. In general, the gain is very sensitive to changes in the matching conditions, which may result in mismatched matching networks. Although higher drain voltages can be seen to increase the gain significantly, the increase can be seen to be diminishing as the voltage increases. This due to the higher power dissipation, which increases the self-heating and hence reduces the gain.

3.2 Temperature Compensation

Envelope tracking optimizes the efficiency by measuring the envelope of the RF input signal to determine the needed bias. Similarly, the supplies can be operated to optimize e.g. the gain or noise at different operating temperatures by using the characteristics in section 3.1. In this case, the measured parameter is the ambient temperature, which is equal to the backside temperature of the MMIC. First, a pre-characterization and modeling of the MMIC is needed to predict the performance for a given operating condition. It is straightforward to fit behavioural models to the measured RF parameters, as is performed in paper [C].

The simultaneous dependence on (V_{gs}, V_{gs}, T_a) of the modelled parameters can be analyzed by plotting fixed values of the parameters as contour lines at different temperatures, as seen in Fig. 3.5. Typically, the goal of temperature compensation techniques is to reduce the temperature coefficient of the gain and ideally have constant gain over a large temperature range. As seen in Fig. 3.5, several bias point exist at each temperature, which yield the specified gain. This allows for one more parameter to be controlled if the contour line of this parameter crosses the gain contour. In this case, the noise figure is selected to be controlled together with the gain, with the aim to have constant

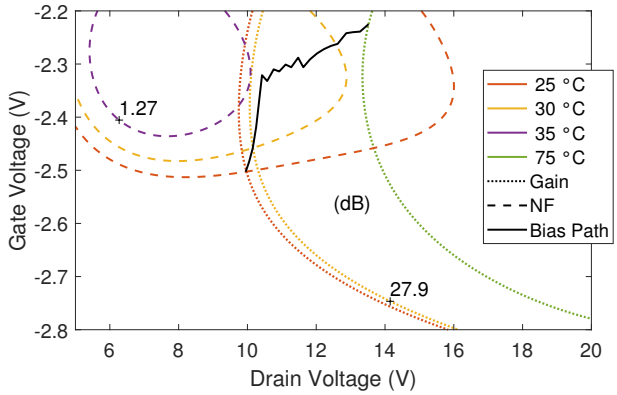

Figure 3.5: Gain and noise figure contours from 25 °C to 75 °C and bias point path to compensate for thermal performance loss.

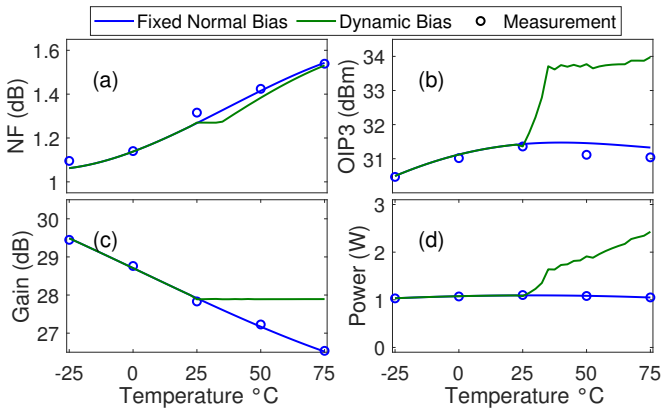

Figure 3.6: Measurement (o) and model (solid lines) of RF parameters versus ambient temperature for fixed recommended bias and dynamic temperature compensation bias. The dynamic bias is performed to maintain the gain and noise level for temperatures above 25 °C.

values above room temperature. Also, since the peak values of the gain and noise occur at different locations in the bias grid, the gain is prioritized as the temperature increases. The bias at each temperature is selected to the intersection point between the gain and NF contour lines. As a result the bias points follow the solid black line in Fig. 3.5.

The parameter behaviour of the LNA can be seen in Fig. 3.6a-d for the recommended bias point and temperature compensation (dynamic) bias. As expected, the gain is constant above 25 °C and the noise is only shortly constant because the increase of thermal noise is much larger than what can be compensated for. Furthermore, it can be seen that the compensation increases the power consumption as the temperature increases. This would also increases the channel temperature, which ultimately reduces the MTTF. Thus, this type of control scheme is not for long term usage, rather for temporarily increasing the device performance. It is however worth mentioning that the power consumption of the LNA can also be controlled to not exceed a certain value, although

tradeoffs with linearity and noise has to be made. The linearity is in this case significantly improved (Fig. 3.6(b)) with a larger gate voltage (Fig. 3.5). For high input powers, this can be used to minimize the nonlinear distortion from the circuit and hence increase the output signal-to-noise and distortion ratio (see paper [a]).

Chapter 4

Conclusions

It is reasonable to assume that GaN-based technologies will be increasingly used for electronic applications. As a result of the high power per unit area, self-heating is today the single most limiting factor for the technology. It is primarily a task for thermal management technologies to solve. However, the characterization techniques play a key role in the development of new cooling solutions. This thesis primarily covers problems regarding electric-based measurements of the thermal resistance, as well as techniques to characterize the laterally coupled heat.

Due to the pronounced effect of electron trapping in GaN, it is useful with a methodology that identifies preconditions, where trapping effects are minimized, and self-heating is maximized. Differential resistance measurements is one method to detect such conditions and hence facilitates the extraction of the thermal resistance. Normally self-heating is the dominating effect, however, [A] shows that this is not always the case. The characterization methodology therefore provides a useful assessment tool for new epitaxial- and substrate topologies. Another area of interest is packaging, where the MMIC is fully enclosed. In this case, the thermal resistance can only be measured with electrical methods, however, the electrical properties may also be affected because of piezoelectric strain induced on the enclosed surface.

GaN technology inherently allows for further circuit miniaturization and facilitates the implementation of high power devices at high frequencies. In these situations, the extent and mechanisms of the laterally coupled heat becomes increasingly important to study. The developed test structure and method in paper [B] is a novel approach to electrically characterize the heat coupling. The compact version of the structure (paper [b]) enables an integration in process control monitoring areas of MMIC processes. The modeling of the transient lateral measurement is of particular interest since it can be used to synthesize a thermal circuit model, which can be used for thermal simulations in conventional MMIC design software. Interestingly, one time constant is sufficient to model the coupling over large distances while several are needed for short distances. In general, factors such as the substrate thickness and backside conditions can be assumed to strongly influence the transient response.

Although it is more complex to implement a dynamic bias control of the drain, measurements show its need to compensate e.g. gain loss. Utilizing both

the gate and drain gives a high degree of freedom, however, tradeoffs between noise, gain, and power consumption are inevitable.

Future Work

A continuation of the covered material in the thesis and additional related studies of interest can be summarized as follows.

- The lateral measurements were limited to only one type of heat source. It therefore remains to study the significance of its size and power but also to evaluate samples with different backside contact (e.g. metallized). In the next step, a lateral study evaluating e.g. the buffer and substrate thickness can be performed. To continue the work towards a complete thermal model, the transient model also needs to be extended to take the separation and operating temperature into account.

- Electrical methods that measures the thermal resistance for different quiescent power levels are not common. The method used in this work is promising but needs further verification for its implementation in GaN. The significance of the type of IV model as well as the parasitic contributions are important to evaluate since it affects the extraction. In addition, a verification with other electrical and optical temperature measurements is needed. The next step is to evaluate a scaled up, high power GaN resistor.

- The differential resistance measurement is a straight forward measurement to quantify electron trapping. In particular, the impact off trapping on the sheet resistivity can be more isolated if the width of the resistor is decreased to reduce the heating. Measurements above 100 °C are also needed since the the discrepancy between the long and short resistors is expected to be reduced at higher temperatures.

- The thermal compensation technique is an initial step towards an advanced bias control system for microwave amplifiers. To make the demonstrated technique viable for real applications, the frequency dependence should also be considered. It is also of interest to investigate how the variations between several LNAs impacts the generality of the models.

- There are several types of packages and cooling solutions where the electrothermal methods come well in hand. Integrated heat-spreaders on the top of the GaN die, mounted either directly or with e.g. metal pillars, is one area of interest. Packaging techniques, which utilize top side cooling has the possibility to create a cheap cooling solution for GaN applications without requiring changes to the technology process.

Acknowledgments

I would like to express my gratitude to those who has contributed directly or indirectly to this work.

This research has been carried out in the GigaHertz centre in a joint research project financed by Swedish Governmental Agency of Innovation Systems (VINNOVA), Chalmers University of Technology, Ericsson AB, Saab AB, Infineon Technologies AG, Keysight Technologies, and United Monolithic Semiconductors.

This work was also performed within the Competence Center for III-Nitride Technology C3Nit-Janzén and has received financial support from the Swedish Governmental Agency for Innovation Systems (VINNOVA) via grant No. 2016-05190, Linköping University, Chalmers University, ABB, Epiluvac, Ericsson, FMV, Gotmic, On Semiconductor, Saab, SweGaN, and United Monolithic Semiconductors (UMS).

Bibliography

[1] "Ericsson Mobility Report," Ericsson AB, Tech. Rep., November 2019.

[2] "Ericsson Technology Review," Ericsson AB, Tech. Rep., February 2017.

[3] Y. Tang, K. Shinohara, D. Regan, A. Corrion, D. Brown, J. Wong, A. Schmitz, H. Fung, S. Kim, and M. Micovic, "Ultrahigh-Speed GaN High-Electron-Mobility Transistors With $f_T/f_{\max}$ of 454/444 GHz," *Electron Device Lett.*, vol. 36, no. 6, pp. 549–551, June 2015.

[4] K. Makiyama, S. Ozaki, T. Ohki, N. Okamoto, Y. Minoura, Y. Niida, Y. Kamada, K. Joshin, K. Watanabe, and Y. Miyamoto, "Collapse-free high power InAlGaN/GaN-HEMT with 3 W/mm at 96 GHz," in *IEEE Int. Electron Devices Meeting*, Dec. 7-9, 2015, pp. 9.1.1–9.1.4.

[5] M. Kuzuhara and H. Tokuda, "Low-Loss and High-Voltage III-Nitride Transistors for Power Switching Applications," *IEEE Trans. Electron Devices*, vol. 62, no. 2, pp. 405–413, Feb. 2015.

[6] R. Quay, *Gallium Nitride Electronics.* Germany: Springer, Berlin, Heidelberg, 2008.

[7] R. Guggenheim and L. Rodes, "Roadmap Review for Cooling High-power GaN HEMT Devices," in *IEEE Int. Conf. on Microwaves, Antennas, Communications and Electronic Systems*, Nov. 13-15, 2017, pp. 1–6.

[8] Y. Wu, M. Moore, A. Saxler, T. Wisleder, and P. Parikh, "40-W/mm Double Field-plated GaN HEMTs," in 64^{th} *Device Research Conf.*, June 26-28, 2006, pp. 151–152.

[9] J. Pomeroy, N. Rorsman, J. Chen, U. Forsberg, E. Janzen, and M. Kuball, "Improved GaN-on-SiC Transistor Thermal Resistance by Systematic Nucleation Layer Growth Optimization," in *IEEE Compound Semiconductor Integrated Circuit Symposium*, Oct. 13-16, 2013, pp. 1–4.

[10] S. Nuttinck, B. K. Wagner, B. Banerjee, S. Venkataraman, E. Gebara, J. Laskar, and H. M. Harris, "Thermal analysis of AlGaN-GaN power HFETs," *IEEE Trans. Microw. Theory Techn.*, vol. 51, no. 12, pp. 2445–2452, Dec. 2003.

[11] D. Gómez, C. Dufis, J. Altet, D. Mateo, and J. L. González, "Electro-thermal coupling analysis methodology for rf circuits," *Microelectronics Journal*, vol. 43, no. 9, pp. 633 – 641, Sep. 2012.

[12] A. Chini, F. Soci, M. Meneghini, G. Meneghesso, and E. Zanoni, "Deep Levels Characterization in GaN HEMTs—Part II: Experimental and Numerical Evaluation of Self-Heating Effects on the Extraction of Traps Activation Energy," *IEEE Trans. Electron Devices*, vol. 60, no. 10, pp. 3176–3182, Oct. 2013.

[13] T. H. Yu and K. F. Brennan, "Monte Carlo calculation of two-dimensional electron dynamics in GaN-AlGaN heterostructures," *J. Appl. Phys.*, vol. 91, no. 6, pp. 3730–3736, March 2002.

[14] M. S. Pramanick and A. Ghosal, "Effects of Scattering on Transport Properties in GaN," in *Devices for Integrated Circuit*, March 23-24, 2017, pp. 647–651.

[15] L. Ardaravičius, A. Matulionis, J. Liberis, O. Kiprijanovic, M. Ramonas, L. F. Eastman, J. R. Shealy, and A. Vertiatchikh, "Electron drift velocity in AlGaN/GaN channel at high electric fields," *Appl. Phys. Lett.*, vol. 83, no. 19, pp. 4038–4040, Nov. 2003.

[16] C. Potier, A. Martin, M. Campovecchio, S. Laurent, R. Quere, J. C. Jacquet, O. Jardel, S. Piotrowicz, and S. Delage, "Trap Characterization of Microwave GaN HEMTs Based on Frequency Dispersion of the Output-Admittance," in 9^{th} *European Microwave Integrated Circuit Conf.*, Oct. 6-7, 2014, pp. 464–467.

[17] J. Fang, M. V. Fischetti, R. D. Schrimpf, R. A. Reed, E. Bellotti, and S. T. Pantelides, "Electron Transport Properties of $Al_xGa_{1-x}N$/GaN Transistors Based on First-Principles Calculations and Boltzmann-Equation Monte Carlo Simulations," *Phys. Rev. Applied*, vol. 11, no. 4, p. 044045, Apr. 2019.

[18] S. A. Vitusevich, S. V. Danylyuk, N. Klein, M. V. Petrychuk, A. Y. Avksentyev, V. N. Sokolov, V. A. Kochelap, A. E. Belyaev, V. Tilak, J. Smart, A. Vertiatchikh, and L. F. Eastman, "Separation of hot-electron and self-heating effects in two-dimensional AlGaN/GaN-based conducting channels," *Appl. Phys. Lett.*, vol. 82, no. 5, pp. 748–750, Feb. 2003.

[19] G. Meneghesso, F. Zanon, M. J. Uren, and E. Zanoni, "Anomalous Kink Effect in GaN High Electron Mobility Transistors," *IEEE Electron Device Lett.*, vol. 30, no. 2, pp. 100–102, Feb. 2009.

[20] K. R. Bagnall, O. I. Saadat, S. Joglekar, T. Palacios, and E. N. Wang, "Experimental Characterization of the Thermal Time Constants of GaN HEMTs Via Micro-Raman Thermometry," *IEEE Trans. Electron Devices*, vol. 64, no. 5, pp. 2121–2128, May 2017.

[21] K. Maize, G. Pavlidis, E. Heller, L. Yates, D. Kendig, S. Graham, and A. Shakouri, "High Resolution Thermal Characterization and Simulation of Power AlGaN/GaN HEMTs Using Micro-Raman Thermography and 800 Picosecond Transient Thermoreflectance Imaging," in *IEEE Compound Semiconductor Integrated Circuit Symp.*, Oct. 19-22, 2014, pp. 1–8.

[22] A. Sarua, Hangfeng Ji, M. Kuball, M. J. Uren, T. Martin, K. P. Hilton, and R. S. Balmer, "Integrated Micro-Raman/Infrared Thermography Probe for Monitoring of Self-Heating in AlGaN/GaN Transistor Structures," *IEEE Trans. Electron Devices*, vol. 53, no. 10, pp. 2438–2447, Oct. 2006.

[23] J. Christofferson, K. Maize, Y. Ezzahri, J. Shabani, X. Wang, and A. Shakouri, "Microscale and Nanoscale Thermal Characterization Techniques," in *Int. Conf. on Thermal Issues in Emerging Technologies: Theory and Application*, Jan. 3-6, 2007, pp. 3–9.

[24] D. Kendig, G. Pavlidis, S. Graham, J. Reiter, M. Gurr, D. Altman, S. Huerster, and A. Shakouri, "UV Thermal Imaging of RF GaN Devices with GaN Resistor Validation," in *91st ARFTG Microwave Measurement Conf.*, June 15, 2018, pp. 1–4.

[25] D. L. Blackburn, "Temperature Measurements of Semiconductor Devices - A Review," in 20^{th} *Annu. IEEE Semiconductor Thermal Measurement and Management Symp.*, March 11, 2004, pp. 70–80.

[26] O. Arenas, . A. Alam, A. Chakroun, V. Aimez, A. Jaouad, R. Ares, F. Boone, and H. Maher, "Thermal Performance Assessment in AlGaN/GaN Structures by Microsensor Integration," in 10^{th} *European Microwave Integrated Circuits Conf.*, Sep. 7-8, 2015, pp. 227–230.

[27] F. Cozette, M. Lesecq, A. Cutivet, N. Defrance, M. Rousseau, H. Maher, and J. C. De Jaeger, "NResistive Nickel Temperature Sensor Integrated Into Short-Gate Length AlGaN/GaN HEMT Dedicated to RF Applications," *IEEE Electron Device Lett.*, vol. 39, no. 10, pp. 1560–1563, Oct. 2018.

[28] M. Wu, X. Ma, L. Yang, Q. Zhu, M. Zhang, L. Yang, and Y. Hao, "Accurate Measurement of Channel Temperature for AlGaN/GaN HEMTs," *IEEE Trans. Electron Devices*, vol. 65, no. 11, pp. 4792–4799, Nov. 2018.

[29] J. Joh, J. A. del Alamo, U. Chowdhury, T. Chou, H. Tserng, and J. L. Jimenez, "Measurement of Channel Temperature in GaN High-Electron Mobility Transistors," *IEEE Trans. Electron Devices*, vol. 56, no. 12, pp. 2895–2901, Dec. 2009.

[30] G. Pavlidis, S. Pavlidis, E. R. Heller, E. A. Moore, R. Vetury, and S. Graham, "Characterization of AlGaN/GaN HEMTs Using Gate Resistance Thermometry," *IEEE Trans. Electron Devices*, vol. 64, no. 1, pp. 78–83, Jan. 2017.

[31] A. M. Darwish, A. J. Bayba, and H. A. Hung, "Utilizing Diode Characteristics for GaN HEMT Channel Temperature Prediction," *IEEE Trans. Microw. Theory Techn.*, vol. 56, no. 12, pp. 3188–3192, Dec. 2008.

[32] A. Cutivet, F. Cozette, M. Bouchilaoun, A. Chakroun, O. Arenas, M. Lesecq, J. De Jaeger, A. Jaouad, F. Boone, and H. Maher, "Characterization of Dynamic Self-Heating in GaN HEMTs Using Gate Resistance Measurement," *IEEE Electron Device Lett.*, vol. 38, no. 2, pp. 240–243, Feb. 2017.

[33] A. Cutivet, M. Bouchilaoun, B. Hassan, C. Rodriguez, A. Soltani, F. Boone, and H. Maher, "Thermal Transient Extraction for GaN HEMTs by Frequency-Resolved Gate Resistance Thermometry with Sub-100 ns Time Resolution," *Phys. Status Solidi (a)*, vol. 216, no. 1, p. 1800503, Jan. 2019.

[34] D. G. Cahill, "Thermal conductivity measurement from 30 to 750 K: the 3ω method," *Rev. Sci. Instrum.*, vol. 61, no. 2, pp. 802–808, Feb. 1990.

[35] M. Avcu, R. Sommet, J. Teyssier, G. Callet, A. El-Rafei, and R. Quéré, "Measurement of thermal impedance of GaN HEMTs using 3ω method," *Electron. Lett.*, vol. 48, no. 12, pp. 708–710, June 2012.

[36] A. Mustafa, S. Raphael, and Q. Raymond, "Influence of Parasitic Effects of the "3ω" Measurement Setup to Improve the Determination of GaN HEMTs Thermal Impedance," in 9^{th} *European Microwave Integrated Circuit Conf.*, Oct. 6-7, 2014, pp. 9–12.

[37] K. Andersson, C. Fager, and J. C. Pedro, "A general procedure for extraction of bias dependent dynamic self heating model parameters," in *IEEE MTT-S Int. Microwave Symp. Dig.*, June 17, 2005, pp. 1159–1162.

[38] E. McCune, "Fundamentals for Energy-Efficient Massive MIMO," in *IEEE Wireless Communications and Networking Conf. Workshops*, March 19-22, 2017, pp. 1–6.

[39] M. Thorsell, K. Andersson, H. Hjelmgren, and N. Rorsman, "Electrothermal Access Resistance Model for GaN-Based HEMTs," *IEEE Trans. Electron Devices*, vol. 58, no. 2, pp. 466–472, Feb. 2011.

[40] A. Sommerfeld, *Introduction to Partial Differential Equations.* New York, USA: Academic Press, 1949.

[41] H. Shibata, Y. Waseda, H. Ohta, K. Kiyomi, K. Shimoyama, K. Fujito, H. Nagaoka, Y. Kagamitani, R. Simura, and T. Fukuda, "High Thermal Conductivity of Gallium Nitride (GaN) Crystals Grown by HVPE Process," *Material Transactions*, vol. 48, no. 10, pp. 2782–2786, Sep. 2007.

[42] Q. Qi and Z. Chen, "A K -Band CMOS Amplifier With Temperature Compensation for Gain Variation Reduction," *IEEE Microw. Compon. Lett.*, vol. 28, no. 2, pp. 150–152, Feb. 2018.

[43] D. Gomez, M. Sroka, and J. L. G. Gonzalez Jimenez, "Process and Temperature Compensation for RF Low-Noise Amplifiers and Mixers," *IEEE Trans. Circuits Syst. I, Reg. Papers*, vol. 57, no. 6, pp. 1204–1211, June 2010.

[44] K. Yamauchi, Y. Iyama, M. Yamaguchi, Y. Ikeda, S. Urasaki, and T. Takagi, "X-band MMIC Power Amplifier With an on-chip Temperature Compensation Circuit," *IEEE Trans. Microw. Theory Techn.*, vol. 49, no. 12, pp. 2501–2506, Dec. 2001.

[45] H. Lee, H. Fuad, T. Tan, and T. Low, "A Broadband Flat Gain High Linearity Gain Block MMIC Amplifier with Built-in Temperature Compensation Active Bias Circuitry," in *Asia Pacific Microwave Conf.*, Dec. 7-10, 2009, pp. 349–352.

Paper A

Thermal Characterization of GaN HEMTs Affected by Trapping Effects Using Electrical Measurements

J. Bremer, D. Y. Chen, A. Malko, M. Madel, N. Rorsman, S. E. Gunnarsson, K. Andersson and M. Thorsell

submitted to *IEEE Transactions on Electron Devices*, 2019

Paper B

Analysis of Lateral Thermal Coupling for GaN MMIC Technologies

J. Bremer, J. Bergsten, L. Hanning, T. Nilsson, N. Rorsman, S. Gustafsson A. M. Eriksson and M. Thorsell

***IEEE Transactions on Microwave Theory and Techniques*, vol. 66, no. 10, pp. 4430-4438, October, 2018.**

Paper C

Compensation of Performance Degradation Due to Thermal Effects in GaN LNA Using Dynamic Bias

J. Bremer, L. Hanning, N. Rorsman and M. Thorsell

in *48th European Microwave Conference*, Madrid, September, 2018, pp. 1213-1216.